Global Modeling of Millimeter-Wave Circuits: Electromagnetic Simulation of Amplifiers

S. M. S. Imtiaz, *Member, IEEE,* and Samir M. El-Ghazaly, *Senior Member, IEEE*

***Abstract*—Global modeling of microwave and millimeter-wave circuits is important to simulate the electromagnetic (EM) coupling, device-EM wave interaction, and the EM radiation effects of the closely spaced active and passive components of monolithic microwave integrated circuits (MMIC's). In this paper, a global-modeling technique is presented to characterize the millimeter-wave integrated-circuit amplifiers. The characterization of amplifier circuits, including the input and output matching networks, are performed using a full-wave analysis coupled with physical modeling of the semiconductor devices. The entire amplifier is simulated with the finite-difference time-domain (FDTD) algorithm, which also solves for the EM fields inside the transistor. The intensive computer-memory requirement and the large simulation time are reduced by applying a hybridization approach. The small signal as well as the large signal propagation through the amplifier circuit are demonstrated. The scattering parameters are extracted for the amplifier circuit at small and large signals for different frequencies. The global technique is able to model the nonlinearity and the harmonic distortion of the amplifier circuit. The third and fifth harmonic components in the output spectrum at large signal are predicted for different frequencies.**

***Index Terms*—Circuit simulations amplifiers, device modeling, MESFET.**

I. Introduction

THE increasing demand of processing and transmitting more information at a faster rate drives the analog and digital electronic systems to operate at higher frequencies or higher clock speeds. At the same time, to curtail the production cost, the manufacturers are more inclined toward heavily dense integrated circuits. In these high-density integrated circuits, there are many closely spaced active and passive devices. As a result, there are some detrimental effects on the circuit performance at high frequencies due to crosstalk caused by coupling, surface waves, and radiation effects. In such cases, the circuit modeling issue becomes more intensive. The circuit design should be based on the advanced global model, which takes the electromagnetic (EM) wave effects into consideration. This global model will analyze all the circuit elements concurrently, taking into account the EM coupling, radiation effects, and electron–wave interaction. More effects which are traditionally viewed to be secondary, such as thermal and packaging effects, may be included in the global modeling to enhance the accuracy. However, this may be achieved in the future as the comprehensive global-modeling concept develops. On the other hand, in the device level, the exciting development in semiconductor technology over the last three decades have led to an increasing demand to model semiconductor devices. With the ever decreasing device dimensions, the researchers developed some state-of-the-art techniques for their analysis, design, and optimization. The velocity overshoot phenomenon, hot electron, and quantum mechanical effects were taken into consideration in these techniques.

The global-modeling technique is still a new concept in its essence. In this technique, the active devices are simulated by combining the electron transport and the EM models. The passive devices are simulated using the EM model. We have already developed a combined EM and solid-state (CESS) simulator for the analysis of high-frequency MESFET's [1]. The CESS simulator couples a semiconductor model to the three-dimensional (3-D) time-domain solution of Maxwell's equations using the finite-difference time-domain (FDTD) algorithm. The semiconductor model is based on the moments of the Boltzmann transport equation. The EM model is required at high frequencies to simulate the device behavior in those situations when the wave period of the propagating EM signal becomes proportional to the electron relaxation times, and the wavelength is comparable to the device width. The resulting electron–wave interaction is taken into consideration using the CESS model. This model can predict the nonlinear energy buildup inside the transistor. The other advantage is its ability to show the dispersive nature of the device, especially at high frequencies. While connecting the closely spaced passive and active circuits, the EM coupling and the radiation effects can be simulated employing the EM model as well.

The hybridization technique in monolithic microwave integrated circuits (MMIC's) was previously used in coupling the lumped elements and the distribution network of the transmission lines in many different forms [2]–[6]. Some works were done for hybrid systems with active and passive lumped elements by the FDTD [7] and TLM methods [8], [9]. The technique was applied to simulate the picosecond pulse generation by an optically excited GaAs devices using 3-D charge transport models [10], [11]. Some researchers modeled the three-terminal active devices by incorporating two-terminal lumped elements into several FDTD subgrids [12], [13] and by using the SPICE lumped circuits in the FDTD solution of Maxwell's equation [14]. The microwave amplifiers were

Manuscript received March 31, 1997; revised August 15, 1997. This work was supported by the U.S. Army Research Office under contract DAAH04-95-1-0252.

S. M. S. Imtiaz is with Micro Linear Corporation, San Jose, CA 95131 USA.

S. M. El-Ghazaly is with the Department of Electrical Engineering, Telecommunications Research Center, Arizona State University (ASU), Tempe, AZ 85287-7206 USA (e-mail: sme@asu.edu).

Publisher Item Identifier S 0018-9480(97)08321-X.

simulated by using the equivalent voltage- and current-source approaches for the transistor [15], [16]. The characterization of microwave circuits containing various lumped components was performed using a global EM analysis [17]. In [7]–[17], the physical devices were not simulated—the lumped elements were used instead. This process of replacing the active device with the equivalent sources or the equivalent circuit parameters may not represent all aspects of device nonlinearity and wave–device interactions at the millimeter-wave frequencies. The alternative approach is to simulate the integrated circuit by coupling the physical equations representing the semiconductor device with the EM fields in the transmission lines with an accurate FDTD algorithm. However, the FDTD method requires intensive computer memory and consumes a considerable amount of time for its operation.

The problem of large computer memory and time can be reduced by breaking a circuit into subcircuits, then solving them individually and reconnecting them together. This method was successfully applied to steady-state networks [18], [19] and to time-domain solutions using the transmission-line matrix (TLM) [20], [21]. The computer-memory requirements were reduced by Prony's method [22], [23] and by system identification technique [24], [25]. A suitable technique can be applied to the simulation to reduce the computer time and memory requirements.

In this paper, the global-modeling technique is applied to a millimeter-wave amplifier with the input and output matching networks to demonstrate its potential. Although the global modeling is a simply conceivable technique, its implementation is not easy in the amplifier circuit. There are several constraints which make the implementation very difficult. Besides the computer-memory requirements and large simulation time, the other issues, such as the numerical stability and accuracy for modeling different circuit components, diversified device dimensions, different physical and EM aspects of the devices, and circuits play a very important role as well. The global model needs to take care of these aspects. For example, in the amplifier, the input and the output matching networks are very large compared to the transistor. However, the mesh size and, consequently, the FDTD stability criteria for the amplifier, are severely limited by the Debye length of the semiconductor. This imposes a constraint on the time step Δt of the FDTD algorithm, which becomes of the order of 10^{-17} s. If the input and the output matching networks were to be simulated using this criteria, it would take such a long time to simulate the amplifier circuit that it becomes almost impossible using the current computers.

To avoid these problems, the millimeter-wave amplifier with the matching networks is divided into three regions. The physical characteristics of the amplifier circuit are preserved by incorporating a simple, but rigorous, hybridization technique. The full-wave analysis of each region is individually performed and properly coupled to the next stage with all the required informations from the preceding stage. This technique enables one to use large space step, and hence, large time step in matching networks. The computer simulation time is drastically reduced compared to the method incorporating the nonuniform mesh for the whole amplifier. The computer memory requirement is also lowered by approximately 66% at a certain time. This model can show the small and the large signal responses of the amplifier, the frequency contents of the output spectrum, nonlinearity, and distortion in the time-domain responses at large signal. These characteristics are more vivid in this global model than any other simulators. The amplifier analysis, coupling procedure, and results are summarized in the following sections.

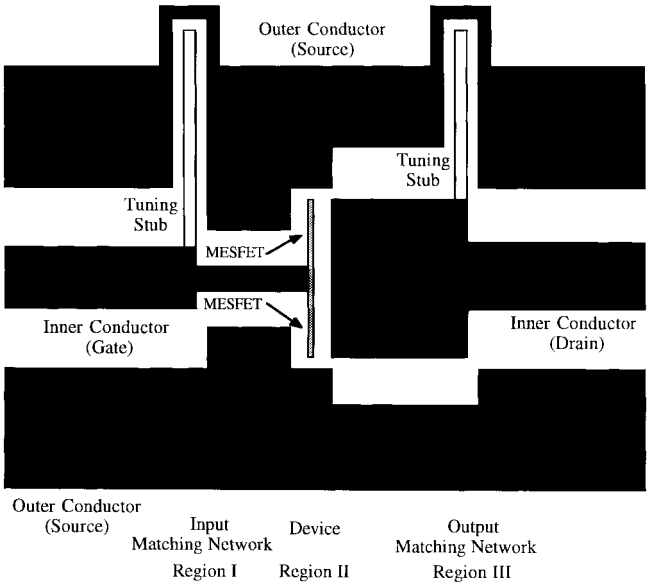

Fig. 1. GaAs transistor amplifier with matching networks.

II. Analysis of the Amplifier

As a step toward global modeling of millimeter-wave circuits, a complete amplifier implemented in a coplanar waveguide (CPW) configuration is simulated. The amplifier along with the matching networks is shown in Fig. 1. The input and the output matching networks are designed based on the s-parameters of the transistor. The transistor channel length and aspect ratio are selected to achieve the required transconductance and the cutoff frequency. The dc analysis was performed for the MESFET shown in Fig. 2. The cutoff frequency of the device was estimated as 77 GHz. The operating frequency is chosen to be 40 GHz to illustrate the principle of the approach. The scattering parameters are computed for the MESFET at the selected bias point. The equivalent circuit admittances of the MESFET are obtained from the simulated s-parameters.

The dimensions of the center and outer conductors of the matching networks are selected to achieve a characteristic impedance of about 50-Ω and to connect them perfectly at the input and the output sides of MESFET. The line and the stub lengths of the matching networks are designed from the source and the load admittances of the MESFET.

III. Coupling the Matching Networks to the Transistor

The millimeter-wave amplifier is divided into three regions. The simulation of each region is separately performed and

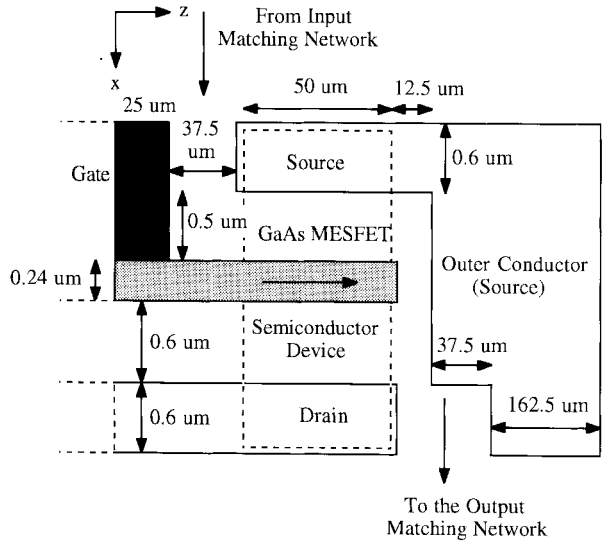

Fig. 2. The top view of one half of the GaAs MESFET structure.

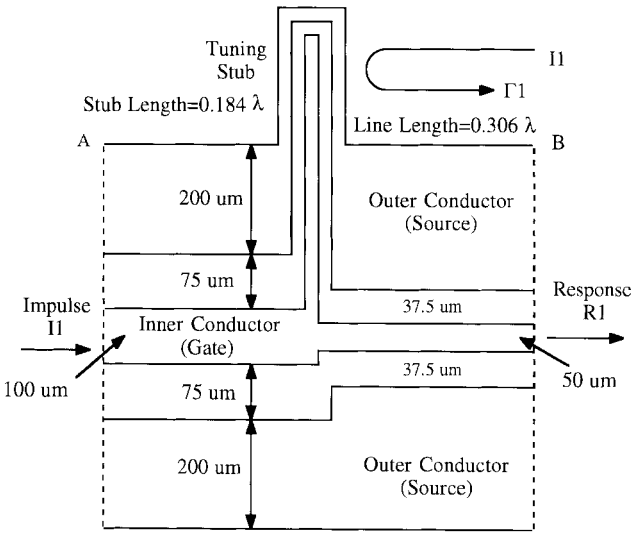

Fig. 3. The input matching network.

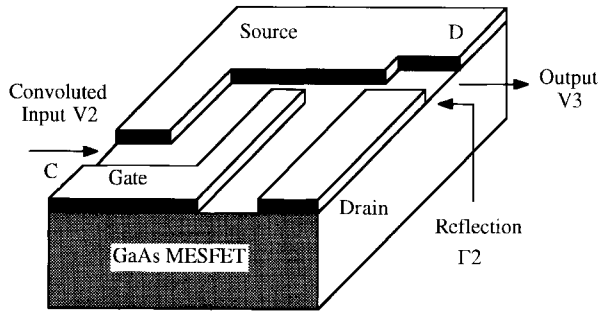

Fig. 4. Coupling in GaAs MESFET.

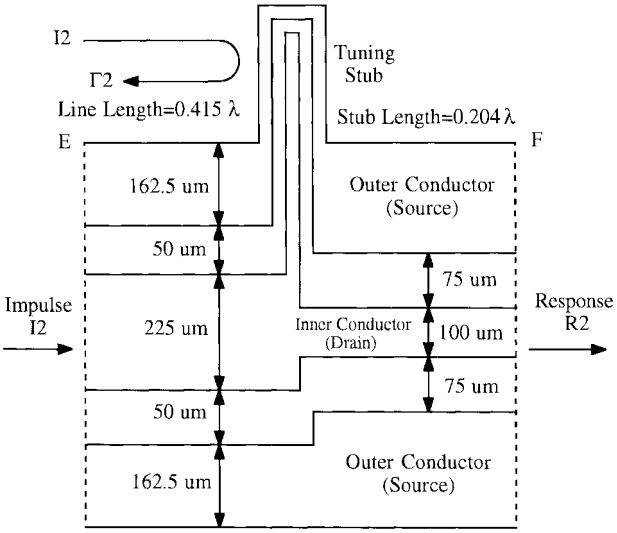

Fig. 5. The output matching network.

properly coupled to the next stage with all the required informations of the preceding stage. At the input of Region I, an impulse I_1 is applied. The EM model is solved for the input matching network using the FDTD algorithm. The response R_2 is collected at point B, as shown in Fig. 3. The reflection coefficient Γ_1 of Region I is obtained by applying the same impulse at point B. When the impulse is incident at B, part of it is transmitted and the rest is reflected back. The reflected wave is identified and the time dependent Γ_1 is obtained.

A sinusoidal wave is applied to the amplifier input. The response V_2 to the sine wave can be obtained by summing up the impulse responses convoluted in time with proper magnitudes. The signal V_2 is now applied to the transistor, as shown in Fig. 4. The CESS simulator is used to propagate this signal. The reflected wave V_{R1} from the MESFET is identified and convoluted with the reflection coefficient Γ_1 and the resulting signal is also added to V_2. Thus, at point C the applied ac voltage is

$$V_C(t) = V_2(t) + \sum \Gamma_1(\tau) \cdot V_{R1}(t-\tau). \tag{1}$$

The reflection coefficient Γ_2 for an impulse I_2 at the output matching network is obtained (Fig. 5). The Γ_2 is convoluted with the output of MESFET and is applied as a secondary source at point D. The output wave V_3 is collected in between the drain and the source at point D.

As stated earlier, in Region III an impulse I_2 is applied at input E of the output matching network, as shown in Fig. 5. The EM model is solved in this region. The response R_2 is collected at point F. The wave V_3 can be decomposed to a number of narrow pulses. Thus, the output wave at point F is calculated by convoluting the impulse response R_2 with proper magnitudes.

The flowchart in Fig. 6 illustrates the sequence of operations involved in the solution of EM model in Region I. The same flowchart can be used for Region III. The flowchart in Fig. 7 describes the sequences involved in calculating the time-dependent reflection coefficient Γ_1 in Region I. The same flowchart can be used for the reflection coefficient Γ_2 of Region III at point E. The flowchart for the calculation steps and the coupling procedure between the semiconductor and the EM models in the GaAs MESFET can be found in [1]. The time-domain solution of the EM model is obtained using a 3-D mesh where field components are arranged following

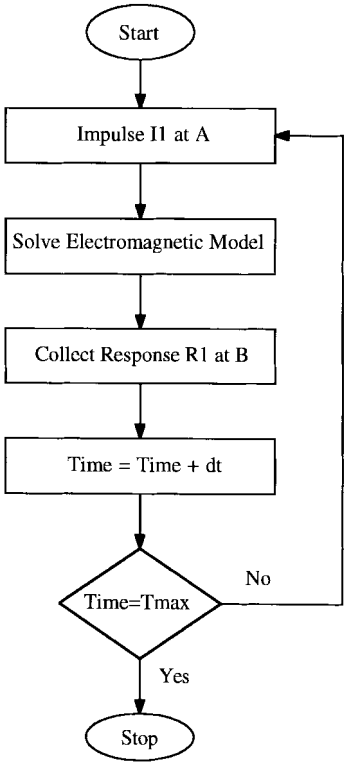

Fig. 6. Flowchart for the solution of the EM model in the matching network.

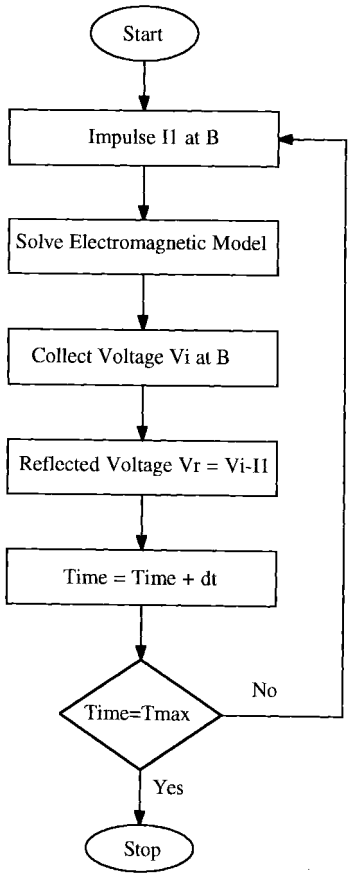

Fig. 7. Flowchart for the reflection coefficient in the matching network.

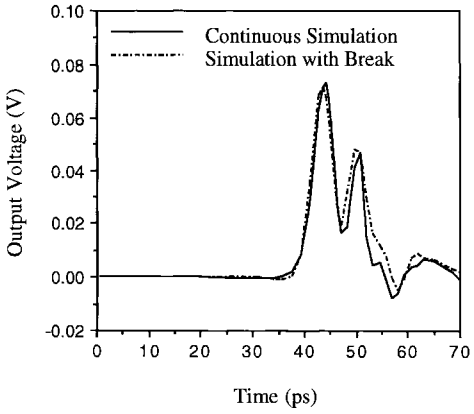

Fig. 8. Comparison of the output voltages for continuous simulation and the simulation with cut. The convolution of impulse response is done in the input matching network only.

Yee's method [26]. Higdon's second-order boundary conditions are used to prevent the reflections from all the sides [27]. The FDTD simulation is performed in a massively parallel (MasPar) super-computer MP2.

In this demonstration, sinusoidal signals are applied to the amplifier input. It should be noted that this is done to illustrate the concept. In general, any arbitrary waveform can be applied to the amplifier without any significant increase in the computational effort.

IV. Results and Discussions

The hybridization approach in global modeling is first applied to the input and the output matching networks without the MESFET to make sure that the technique works with a reasonable accuracy. The electric-field distributions are investigated for the GaAs MESFET along with the adjacent transmission lines. The s-parameters for the whole amplifier is reported next without any kind of optimization. Then the GaAs MESFET is optimized in terms of channel length, aspect ratio, and the active-layer doping density to obtain better gain characteristics. The line and the stub lengths for the input and the output matching networks are recalculated for the optimized transistor. The s-parameters are extracted at different frequencies for applied small and large signals.

A. Hybridization in Matching Networks

The hybridization technique is applied to a microstrip network similar to what is normally used in amplifier matching networks. No transistors are included since the goal is to verify this technique. The microstrip network is designed for the frequency of 80 GHz. A square pulse of magnitude 0.1 and duration 2.5 ps is applied at the input of the microstrip network. The output voltages in time domain and the transfer functions in frequency domain are compared for the continuous simulation and the simulation with break/cut in Figs. 8–10. In Fig. 8, the solid line represents the output voltage for the continuous simulation. The dashed line provides the output voltage for the case where the convolution of the impulse response is performed in the input matching network only to obtain the actual response. The output voltages are in good

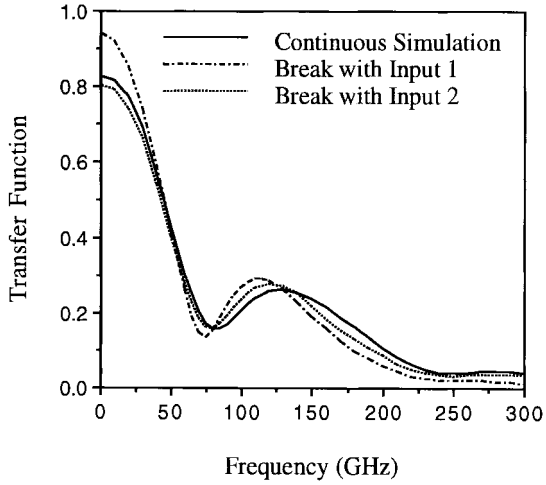

Fig. 9. Comparison of the transfer functions of the microstrip line for continuous simulation and the simulation with cut for two Gaussian pulses. The convolution of impulse response is done in the input matching network only.

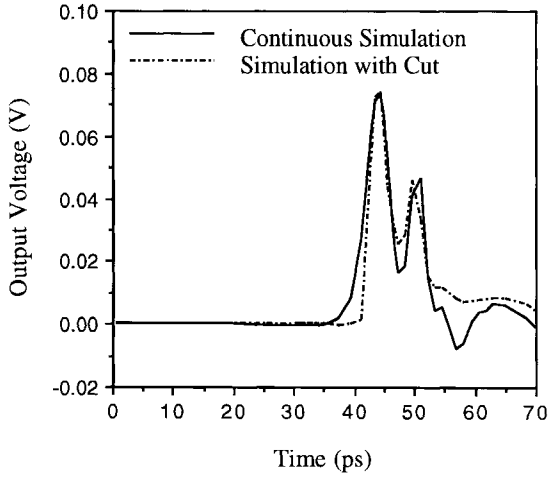

Fig. 10. Comparison of the output voltages for continuous simulation and the simulation with cut. The convolution of impulse response is done in both the matching networks.

agreement with each other. Fig. 9 shows the transfer functions for this case. In this figure, the solid line denotes the transfer function for the continuous simulation. The dashed line with input one means that the Gaussian pulse used as the impulse has a pulsewidth of 0.3 ps and that with input two means that the Gaussian pulse has a pulsewidth of 0.15 ps. While comparing the transfer functions, it is noticed that there exists a global error of 5% in the results between the continuous simulation and the simulation with cut using the impulse of 0.3-ps pulsewidth. The error becomes 1.2% while comparing continuous simulation results with that of the simulation with cut using the impulse of 0.15 ps pulsewidth. This observation explains the source of this error and the solution as well. In this simulation, an impulse was supposed to be applied. Due to the stability problems in computation, a Gaussian pulse of very narrow width was used to obtain the impulse response. The results show that the transfer function with lower Gaussian pulsewidth gives better accuracy. It also indicates that as the pulsewidth is made narrower, a better match is achieved.

In Fig. 10, the output voltages are compared for the continuous simulation and the simulation with cut. In this case, the impulse responses are convoluted in both the matching networks. It means that the response to square pulse in the input matching network is obtained by convoluting the impulse response R_1. Again, the overall response is found by convoluting the impulse response R_2 in the output matching network. A pulsewidth of 0.15 ps is used for the Gaussian pulse. The output voltages are in reasonable agreement with each other.

This process of separately solving for the matching networks requires the computer memory to calculate the impulse responses only once. The results can be used to get the response of any arbitrary input signal with minimum memory requirements. For the results of Figs. 8 and 9, the time needed for the continuous simulation is 223 s and that for the cut is 140 s. Thus, there is a 37% gain in the computational time. On the other hand, for the results of Fig. 10, the time needed for the continuous simulation is 223 s and that for the cut is 58 s. Thus, there is a 74% gain in the computational time. The savings become even more important as the passive part of the amplifier is usually not changed—only the transistor parameters and biasing change. The hybridization approach in global modeling enables one to simulate the amplifier within optimum time.

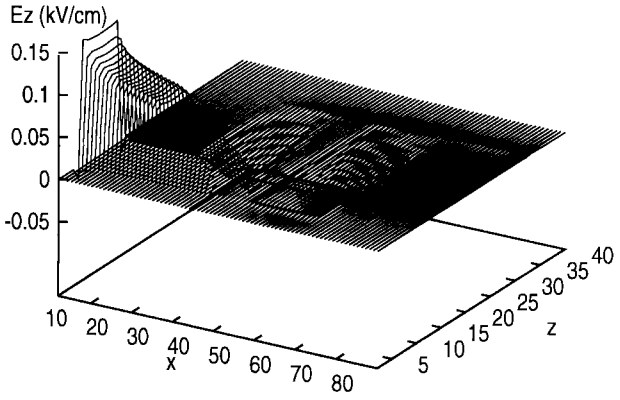

Fig. 11. The electric-field distribution E_z at 2 ps. The electric-field distribution corresponds to the transistor configuration shown in Fig. 4.

B. Electric-Field Distribution

In the transistor portion of the amplifier, only one half of the structure is simulated considering the symmetry. The electric-field distributions at the air–semiconductor interface of the MESFET (Fig. 4) are observed for a Gaussian input. The 3-D electric-field distributions in the z-direction E_z (along the direction of propagation) at the interface are shown in Figs. 11–13 at 2, 4, and 6 ps, respectively. The numbers in the x- and z-axis indicate the mesh points. The mesh spacings in the x- and z-direction are 0.032 μm and 8.13 μm, respectively. At 2 ps, the Gaussian pulse is at its peak. The field is higher at the input side. At 4 ps, the tail of the Gaussian pulse passes through the MESFET. Thus, the decrease in E_z at the input is observed. E_z decreases further at 6 ps. At the same time, the wave propagation is evident from the middle portion of the device.

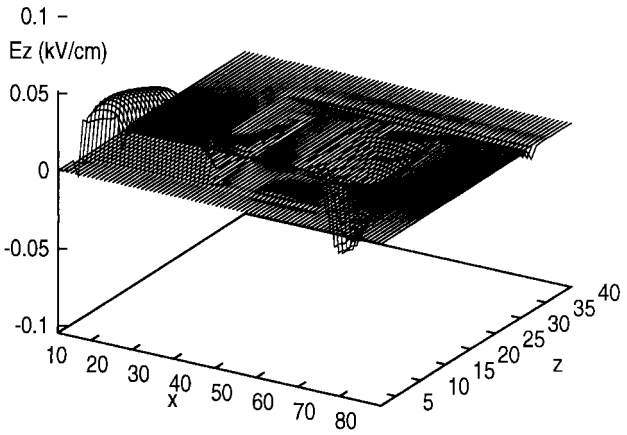

Fig. 12. The electric-field distribution E_z at 4 ps.

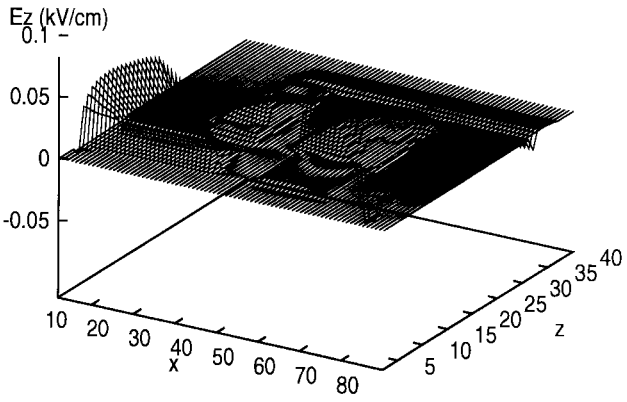

Fig. 13. The electric-field distribution E_z at 6 ps.

C. Simulation of the Amplifier

The amplifier is simulated including the input and the output matching networks. The matching networks are designed for 40-GHz frequency. The GaAs MESFET used here has a gate length $= 0.24$ μm, aspect ratio $= 2.2$ GaAs substrate thickness $= 0.5$ μm, and the active-layer doping $= 2 \times 10^{17}/\text{cm}^3$. The dc operating points are: drain bias $= 3.0$ V and gate bias $= -0.4$ V. A small signal of amplitude 0.1 V is applied to the amplifier. The scattering parameters for the amplifier are obtained at different frequencies. In Fig. 14, S_{21} is shown as a function of frequency. The extraction of S_{21} is performed under simultaneously matched condition. The magnitude of S_{21} remains within a certain range for the frequency band of 20–60 GHz. S_{21} has its peak value at the design frequency, which is expected. The value of S_{21} for this amplifier is low because the transistor width is very small compared to any commercial amplifier. Increasing the transistor width and the aspect ratio would increase the value of S_{21}. In Fig. 15, the variations of S_{12}, S_{11}, and S_{22} are shown with frequency. The magnitude of S_{12} decreases with frequency. The value of S_{12} is small, which is also anticipated. The return loss is less than 25 dB at 40 GHz.

D. Large-Signal Characterization of the Amplifier

Based on the results presented above, another optimized transistor is designed. The GaAs MESFET is optimized in terms of channel length, aspect ratio, and active layer doping to increase the gain characteristics of the amplifier. The drain current is kept the same. The optimized parameters are: gate length $= 0.22$ μm, aspect ratio $= 2.5$, and the active layer doping $= 2.2 \times 10^{17}/\text{cm}^3$. The amplifier is designed for 40-GHz frequency.

The whole amplifier is simulated by applying a small signal of amplitude 0.1 V and large signal of amplitudes 0.3 and 1.0 V. The simulation is performed for 20-, 30-, 40-, 50- and 60-GHz signals. The s-parameters of the amplifier are extracted from the simulation results. In Fig. 16, S_{21} is presented for small and large signals at different frequencies. The large signal s-parameters are calculated at the input signal (i.e., fundamental) frequency. The Fourier transform of the output signal was taken to identify the fundamental from the harmonics. Only the fundamental signal is used. At the design frequency of 40 GHz, the gain is 7.38 dB for small signal and 6.44 and 5.15 dB for large signals of 0.3 and 1.0 V, respectively. Thus, it is observed that for the same design, the gain drops at large signals. In small signal, the gain drops slightly as the frequency is shifted away from the 40-GHz

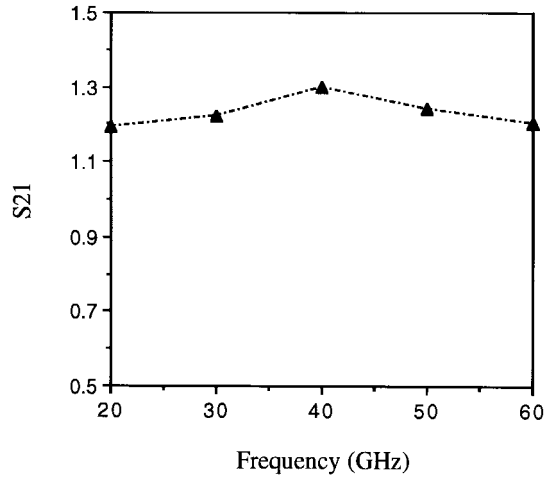

Fig. 14. The dependence of scattering parameter S_{21} on frequency.

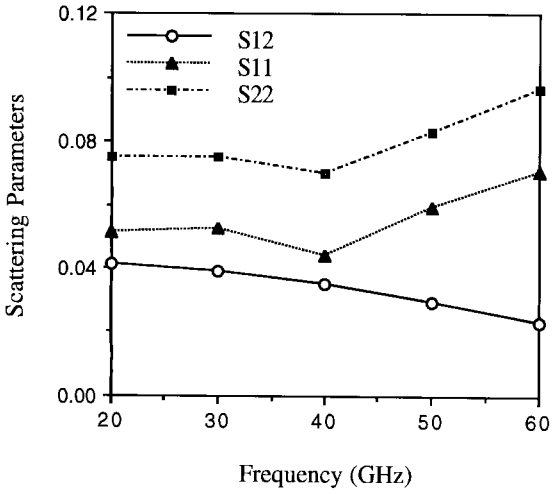

Fig. 15. The variation of scattering parameters S_{12}, S_{11}, and S_{22} with frequency.

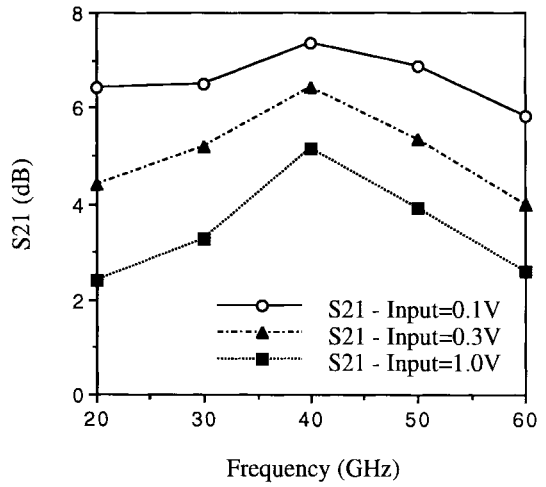

Fig. 16. The dependence of scattering parameters S_{21} on frequency at small and large signals for the amplifier with the optimized transistor.

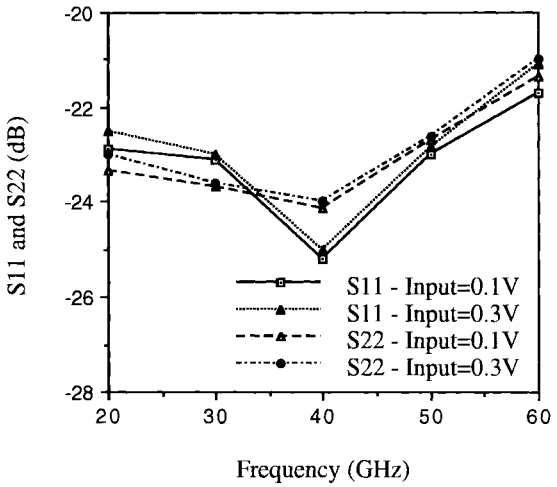

Fig. 18. The dependence of scattering parameters S_{11} and S_{22} on frequency at small and large signals for the amplifier with the optimized transistor.

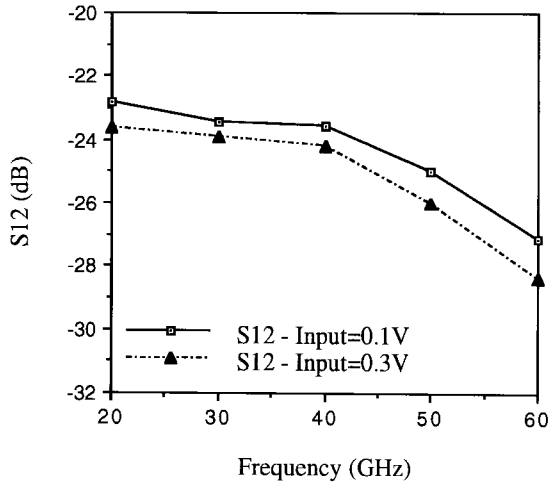

Fig. 17. The variation of scattering parameters S_{12} with frequency at small and large signals for the amplifier with the optimized transistor.

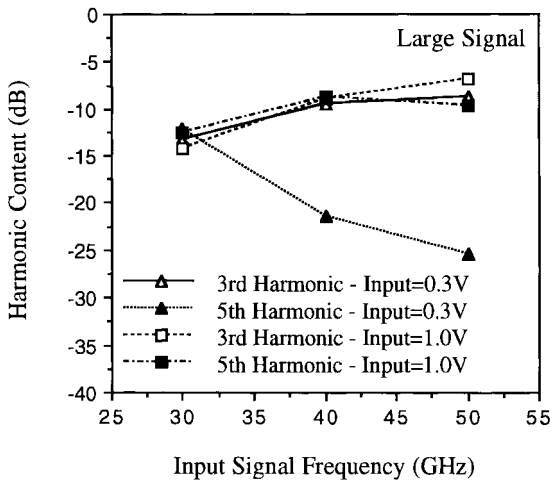

Fig. 19. The harmonic contents with respect to fundamental for the large signal of amplitudes 0.3 and 1.0 V at 30, 40 and 50 GHz.

point. On the other hand, in large signal, the gain reduction at frequencies other than design frequency is higher. Nonlinearity in the device behavior is evident from this figure. It will be seen later that a considerable amount of harmonic power flows in the output. It explains the gain reduction at large signal. The increased harmonic distortion can be considered as the cause of more gain reduction at frequencies other than the design frequency in large signal.

In Fig. 17, the variation of S_{12} is shown for different frequencies. The magnitude of S_{12} is very small as expected and it decreases with frequency. Its magnitude is smaller at large signal. Fig. 18 shows S_{11} and S_{22} for different frequencies at small and large signals. The S_{11} and S_{22} are minimum at the design frequency and increase at other frequencies, which is expected. The return loss is higher for large signals. The difference in magnitude of S_{11} and S_{22} between the small and the large signal increases as the frequency deviates from the design frequency.

Once the large-signal response of the amplifier is obtained, it is interesting to study its frequency content and to identify the harmonics. The output wave contains a significant amount of harmonic components. Besides the fundamentals, the third and fifth harmonic components are strong as well in the output signal. The harmonic contents with respect to fundamental are calculated from the output spectrum at large input signals of 0.3 and 1.0 V at 30, 40, and 50 GHz, shown in Fig. 19. For the large-signal input of 0.3 V, the output power contains 4.8%, 11.6%, and 13% of the fundamental at 30, 40, and 50 GHz, respectively, at the third harmonic. On the other hand, for 1.0-V input signal, the corresponding third harmonic components propagate 3.7%, 12.6% and 21.2% of the fundamental. For the large signal input of 0.3 V, the fifth harmonic contains 6%, 0.7%, and 0.3% of the fundamental at 30, 40, and 50 GHz, respectively. The corresponding fifth harmonic components at input signal of 1.0 V propagate 5.5%, 13.3% and 11% of the fundamental. This shows that a considerable amount of power is transferred at the harmonic components. At 30-GHz signal of amplitude 1.0 V, more higher order harmonics are present. The harmonic distortion is higher for the input signal of 1.0 V. However, it is to be mentioned that for the positive cycle

of 1.0-V input signal, the gate of the transistor is forward-biased which is partially responsible for the higher harmonics generation. Thus, the global model is able to predict the nonlinearity of the device behavior and show the different harmonic components generated at the amplifier output due to nonlinearity. The efficiency of the amplifier at large signal of amplitude 1.0 V is 17.8%, 27.3%, and 20.5% at 30, 40, and 50 GHz, respectively.

The potential of the global-modeling technique is demonstrated in this paper. In an attempt to do this, the millimeter-wave amplifier is simulated by incorporating the EM coupling and device-wave interaction. More effects will be added in the future, including thermal- and EM-radiation effects. By incorporating all these effects in the circuit simulation, we will be able to reach a landmark toward the comprehensive global modeling.

V. Conclusion

An approach toward global modeling of millimeter-wave circuits is presented in this paper. The potential of this approach is demonstrated by applying it to a full-wave characterization of a millimeter-wave amplifier. The amplifier consists of matching networks and a transistor. The EM characteristics of the passive parts are simulated using the FDTD technique. The characteristics of the active part are modeled by coupling the FDTD solution to a physical model of the transistor. The global model is able to characterize the EM coupling, device-EM wave interaction, and the EM radiation effects of the very closely spaced integrated-circuit amplifier.

The hybridization technique, which is used to reduce the computer-memory requirement and the simulation time, is validated by applying it to the amplifier matching networks. The results show a reasonable agreement with the continuous simulation. The electric-field distributions are presented, which shows the flow of the EM wave through the amplifier.

The small-signal, as well as the large-signal wave propagations through the amplifier are analyzed. The amplifier is optimized for a reasonable gain in terms of gate length, aspect ratio, and active layer doping. The s-parameters are extracted for the amplifier circuit at small and large signals for a frequency band of 20–60 GHz. The s-parameters show that the gain drops at large signal and the return loss is higher at large signal. The gain is maximum and the return loss is minimum at the design frequency of 40 GHz. The reduction in gain and the increase in return loss are more at large signal than small signal, as the signal frequency deviates from the design frequency. The global-modeling technique is capable of representing the nonlinearity and the harmonic distortion of the amplifier circuit. A significant third and fifth harmonic components are observed in the output spectrum at large signals for different frequencies.

References

[1] M. A. Alsunaidi, S. M. S. Imtiaz, and S. M. El-Ghazaly, "Electromagnetic wave effects on microwave transistors using a full-wave time domain model," *IEEE Trans. Microwave Theory Tech.*, vol. 44, pp. 799–808, June 1996.

[2] K. Kobayashi, Y. Nemoto, and R. Sato, "Kuroda's identity for mixed lumped and distributed circuits and their application to nonuniform transmission lines," *IEEE Trans. Microwave Theory Tech.*, vol. MTT-29, pp. 81–86, Feb. 1981.

[3] R. M. Cottee and W. T. Joines, "Synthesis of lumped and distributed networks for impedance matching of complex loads," *IEEE Trans. Circuits Syst.*, vol. CAS-26, pp. 316–329, May 1979.

[4] I. Endo, Y. Nemoto, and R. Sato, "Design of transformerless quasi-broad-band matching networks for lumped complex loads using nonuniform transmission lines," *IEEE Trans. Microwave Theory Tech.*, vol. 36, pp. 629–634, Apr. 1988.

[5] Y. Nemoto, K. Kobayashi, and R. Sato, "Equivalent transformations for mixed-lumped Richards section and distributed transmission line," *IEEE Trans. Microwave Theory Tech.*, vol. 36, pp. 635–641, Apr. 1988.

[6] D. Winklestein *et al.*, "Simulation of arbitrary transmission line networks with nonlinear terminations," *IEEE Trans. Circuits Syst.*, vol. 38, pp. 418–422, Apr. 1991.

[7] W. Sui, D. A. Christensen, and C. H. Durney, "Extending the two-dimensional FDTD method to hybrid electromagnetic systems with active and passive lumped elements," *IEEE Trans. Microwave Theory Tech.*, vol. 40, pp. 724–730, Apr. 1992.

[8] R. H. Voelker and R. J. Lomax, "A finite-difference transmission line matrix method incorporating a nonlinear device model," *IEEE Trans. Microwave Theory Tech.*, vol. 38, pp. 302–312, Mar. 1990.

[9] P. Russer, P. P. M. So, and W. J. R. Hoefer, "Modeling of nonlinear active regions in TLM," *IEEE Microwave Guided Wave Lett.*, vol. 1, pp. 10–13, Jan. 1991.

[10] E. Sano and T. Shibata, "Fullwave analysis of picosecond photoconductive switches," *IEEE J. Quantum Electron.*, vol. 26, pp. 372–377, Feb. 1990.

[11] S. M. El-Ghazaly, R. P. Joshi, and R. O. Grondin, "Electromagnetic and transport considerations in subpicosecond photoconductive switch modeling," *IEEE Trans. Microwave Theory Tech.*, vol. 38, pp. 629–637, May 1990.

[12] Y.-S. Tsuei, A. C. Cangellaris, and J. L. Prince, "Rigorous electromagnetic modeling of chip-to-package (first-level) interconnections," *IEEE Trans. Comp., Hybrids, Manufact. Technol.*, vol. 16, pp. 876–883, Dec. 1993.

[13] M. Piket-May, A. Taflove, and J. Baron, "FD-TD modeling of digital signal propagation in 3-D circuits with passive and active loads," *IEEE Trans. Microwave Theory Tech.*, vol. 42, pp. 1514–1523, Aug. 1994.

[14] V. A. Thomas, M. E. Jones, M. Piket-May, A. Taflove, and E. Harrigan, "The use of Spice lumped circuits as sub-grid models for FDTD analysis," *IEEE Microwave Guided Wave Lett.*, vol. 4, pp. 141–143, May 1994.

[15] C.-N. Kuo, V. A. Thomas, S. T. Chew, B. Houshmand, and T. Itoh, "Small signal analysis of active circuits using FDTD algorithm," *IEEE Microwave Guided Wave Lett.*, vol. 5, pp. 216–218, July 1995.

[16] C.-N. Kuo, R.-B. Wu, B. Houshmand, and T. Itoh, "Modeling of microwave active devices using the FDTD analysis based on the voltage-source approach," *IEEE Microwave Guided Wave Lett.*, vol. 6, pp. 199–201, May 1996.

[17] K. Guillouard, M.-F. Wong, V. F. Hanna, and J. Citerne, "A new global finite element analysis of microwave circuits including lumped elements," *IEEE Trans. Microwave Theory Tech.*, vol. 44, pp. 2587–2594, Dec. 1996.

[18] A. Brameller, M. N. John, and M. R. Scott, *Practical Diakoptics for Electrical Networks*. London, U.K.: Chapman & Hall, 1969.

[19] C. R. Brewitt-Taylor and P. B. Johns, "On the construction and numerical solution of transmission-line and lumped network models of Maxwell's equations," *Int. J. Numer. Methods Eng.*, vol. 15, pp. 13–30, 1980.

[20] P. B. Johns and K. Akhtarzad, "The use of time domain diakoptics in time discrete models of fields," *Int. J. Numer. Methods Eng.*, vol. 17, pp. 1–14, 1981.

[21] W. J. R. Hoefer, "The discrete time-domain Green's function or Johns matrix—A new powerful concept in transmission line modeling (TLM)," *Int. J. Numer. Methods Eng.*, vol. 2, pp. 215–225, 1989.

[22] J. L. Dubard, D. Pompei, J. Le Roux, and A. Papiernik, "Characterization of microstrip antennas using the TLM simulation associated with a Prony–Pisarenko method," *Int. J. Numer. Modeling: Electron. Networks, Devices, Fields*, vol. 3, pp. 269–285, 1990.

[23] W. Ko and R. Mittra, "A combination of FD-TD and Prony methods for analyzing microwave integrated circuits," *IEEE Trans. Microwave Theory Tech.*, vol. 39, pp. 2176–2181, Dec. 1991.

[24] W. Kuempel and I. Wolff, "Digital signal processing of time domain field simulation results using the system identification method," in

IEEE MTT-S Int. Symp. Dig., Albuquerque, NM, June 1992, vol. 2, pp. 793–796.
[25] B. Houshmand, T. W. Huang, and T. Itoh, "Microwave structure characterization by a combination of FDTD and system identification methods," *IEEE Microwave Guided Wave Lett.*, vol. 3, pp. 262–264, Aug. 1993.
[26] K. S. Yee, "Numerical solution of initial boundary value problems involving Maxwell's equations in isotropic media," *IEEE Trans. Antennas Propagat.*, vol. AP-14, pp. 302–307, Jan. 1966.
[27] R. L. Higdon, "Numerical absorbing boundary conditions for the wave equation," *Math. Comput.*, vol. 49, pp. 65–91, July 1987.

S. M. S. Imtiaz (S'94–M'96) was born in Dhaka, Bangladesh, in 1966. He received the B.S. and M.S. degrees in electrical engineering from Bangladesh University of Engineering and Technology, Dhaka, Bangladesh, in 1988 and 1990, respectively, and the Ph.D. degree in electrical engineering from Arizona State University (ASU), Tempe, in 1997.

From 1989 to 1991, he was a Lecturer in the Department of Electrical and Electronic Engineering, Bangladesh University of Engineering and Technology. From 1993 to 1997, he was a Teaching/Research Associate in the Department of Electrical Engineering, ASU. In 1997, he joined Micro Linear Corporation, San Jose, CA, as a Senior Device Engineer. His research interests include the modeling and simulation of microwave and millimeter-wave semiconductor devices and circuits, device-wave interactions, numerical techniques, extraction of equivalent circuit parameters of semiconductor devices, and the design, modeling, and simulation of microwave amplifiers.

Dr. Imtiaz is a member of the IEEE Electron Devices Society.

Samir M. El-Ghazaly (S'84–M'88–SM'91) received the Ph.D. degree in electrical engineering from the University of Texas at Austin, in 1988.

In 1988, he was an Assistant Professor with Arizona State University (ASU), Tempe, and became an Associate Professor in 1993. He has also worked at several universities and research centers including the College of Engineering, Cairo University, Cairo, Egypt, as a Teaching Assistant and Assistant Lecturer; the Centre Hyperfrequences et Semiconducteurs, Université de Lille I, France, as a Visiting Professor, working on the simulation of submicron-gate MESFET's; the University of Ottawa, Ottawa, Ont., Canada, as a Summer Faculty Research Fellow, working on millimeter-wave mixers; and CST–Motorola, Inc. (while on leave from ASU), where he worked on modeling semiconductor devices for FT applications. His research interests include microwave lines, wave-device integrations, electromagnetics, and numerical techniques applied to monolithic microwave integrated circuits.

Dr. El-Ghazaly is an elected member of commissions A and D of URSI, a member of Tau Beta Pi, Sigma Xi, and Eta Kappa Nu. He is the secretary of the U.S. National Committee of URSI, Commission A. Since 1991, he has been a member of the Technical Program Committee for the IEEE International Microwave Symposium, and is on the editorial board of the IEEE TRANSACTIONS on MICROWAVE THEORY AND TECHNIQUES. He was the chairman of the IEEE Waves and Devices Group, Phoenix Section, and since 1992, the chapter funding coordinator for IEEE MTT Society. He is currently the chairman of the Chapters Activities Committee of the IEEE MTT Society.